A spectroscopic and computational evaluation of uranyl oxo engagement with transition metal cations

Dominique M. Brager,[a] Ahan J. Panchal,[a] Christopher L. Cahill[a]

[a]*Department of Chemistry, The George Washington University, 800 22nd Street, NW, Washington, DC, 20052, USA.*

Abstract

We report the synthesis and characterization of five novel Cd^{2+}/UO_2^{2+} heterometallic complexes that feature Cd-oxo distances ranging from 78% to 171% of the sum of the van der Waals radii for these atoms. This work marks an extension of our previously reported Pb^{2+}/UO_2^{2+} and Ag^{+}/UO_2^{2+} complexes, yet with much more pronounced structural and spectroscopic effects resulting from Cd-oxo interactions. We observe a major shift in the U=O symmetric stretch and significant uranyl bond length asymmetry. The ρ_{bcp} values calculated using Quantum Theory of Atoms in Molecules (QTAIM) support the asymmetry displayed in the structural data and indicate a decrease in covalent character in U=O bonds with close Cd-oxo contacts; more so than in related compounds containing Pb^{2+} and Ag^{+}. Second Order Perturbation Theory (SOPT) analysis reveals that O sp^x → Cd s is the most significant orbital overlap and U=O bonding and antibonding orbitals also contribute to the interaction (U=O σ/π → Cd d and Cd s → U=O σ/π*). The overall stabilization energies for these interactions were lower than those in previously reported Pb^{2+} cations, yet larger than related Ag^{+} compounds. Analysis of the equatorial coordination sphere of the Cd^{2+}/UO_2^{2+} compounds (along with Pb^{2+}/UO_2^{2+} complexes) reveals that 7-coodinate uranium favors closer, stronger M^{n+}-oxo contacts. These results indicate that U=O bond strength tuning is possible with judicious choice of metal cations for oxo interactions and equatorial ligand coordination.

Introduction

The uranyl cation has long been central to uranium chemistry research owing to its stability in aerobic and aqueous conditions, making it more environmentally relevant and easier to study than more reactive forms of uranium.[1–8] Whereas much research has probed uranyl properties through changes in equatorial ligand coordination, there is also a need to probe the effects of second-sphere interactions. In particular, there is a growing interest in studying interactions with the uranyl oxo groups as they have been shown to promote uranium redox activity which can be leveraged for the purposes of separations or catalysis.[9–14] Of the many possible oxo-interacting species, metal cation-oxo interactions are of particular interest as they have been demonstrated to have significant effects on uranyl electronic structure. [1,15–19] Arnold et al. have extensively studied the effects of M^{n+}-oxo interactions for the purposes of promoting uranyl redox activity by using 'Pac Man' ligand derivatives to engineer close M^{n+}–oxo interactions. By engineering these close contacts they were able to promote significant bond asymmetry indicative of bond weakening.[1,17,20–23] Harder, less polarizable cations, such as Group 1 cations or lanthanides have

even been shown to promote the reduction of U(VI) to U(V) as well as help stabilize the U(V) cation.[20,23–25]

Previous work by our group has expanded on these efforts, offering a spectroscopic perspective, which can inform forensic applications as well as give insight into changes in the molecular orbital construct.[26,27] We have compared the effects of M-oxo interactions with the harder Pb^{2+} cations vs softer Ag^{+} cations on uranyl luminescence and Raman. Close M-oxo contacts with either cation lead to decreased emission intensity and red-shifted U=O symmetric stretches in the Raman. Natural Bond Orbital (NBO) calculations determined that the interaction occurred primarily via charge transfer between acceptor orbitals on the metal cation and donor O sp^x electrons but the U=O σ and U=O σ* orbitals also contributed to the overall interaction. The transfer of electron density within these bonding-relevant orbitals lead to weakening and a loss of covalent character, consistent with red-shifting of the Raman active U=O symmetric stretch. These spectroscopic and bonding effects were stronger in Pb-oxo compounds vs Ag-oxo.

We aim to expand those efforts to the even harder Cd^{2+} cation to determine how spectroscopic signatures and bonding in these complexes may be further affected. Additionally, we aim to probe how differences in equatorial coordination can affect the propensity of the uranyl cation towards forming M^{n+}-oxo interactions. We have synthesized five novel Cd^{2+}/UO_2^{2+} heterometallic complexes, adding to the 20 published in the Cambridge Structural Database.[28] These complexes were characterized structurally, spectroscopically, and computationally to probe the effects of Cd-oxo interactions on bonding and spectroscopic properties. Structural analysis and Raman spectroscopy reveal bond weakening in complexes with closer Cd^{2+}-oxo interactions. Natural Bond Orbital (NBO) analysis reveals that the bond weakening occurs as a result of depopulation of U=O σ/π bonding orbitals and population of U=O σ/π* antibonding orbitals. Evaluation of equatorial bonding suggests that 7-coordinate uranyl compounds are more likely to form oxo-interactions than the 8-coordinate compounds. These efforts describe two approaches by which uranyl oxo-engagement can be tune systematically 1) metal cation hardness 2) equatorial coordination number.

Experimental Section

General. *Caution*: Whereas the uranyl nitrate hexahydrate $[UO_2(NO_3)_2]\cdot 6H_2O$ used in this study consists of depleted U, standard precautions for handling radioactive and toxic substances should be followed.

All organic materials, chelidamic acid monohydrate (chel) (TCI, >95.0%), 2,2';6',2"-terpyridine (terpy) (Sigma Aldrich, 99+%), 1,10-phenanthroline (phen) (Oakwood Chemical, 98%) and 2,2'-bipyridine (bipy) (Sigma Aldrich, 99+%), were purchased and used as received. Cadmium nitrate tetrahydrate (Thermo Scientific, 99+%) is also commercially available and was used without further modification.

Synthesis

All complexes herein were synthesized via hydrothermal methods. The chelidamic acid, N-donor capping ligand, uranyl nitrate, and cadmium nitrate were combined in a 1:1:1:1 ratio. Molar scale, which capping ligands were used, and solvent ratios are outlined in Table 1. Samples were heated at 110°C in a 23 mL Teflon-lined Parr autoclave over 2 days and allowed to cool to room temperature for a few hours before opening. All samples were rinsed with acetone and water. The table below outlines the specifications for the preparation of each compound.

Table 1: Synthesis specifications for the preparation of **1-5**.

Compound	Molar Scale (mol)	Capping Ligand	Solvents
1	0.0003	1,10-phenanthroline	2.25 mL acetonitrile 6.75 mL water
2	0.0001	2,2';6',2"-terpyridine	0.75 mL acetonitrile 2.25 mL water 3.48 mL 0.1M HCl
3	0.0001	2,2';6',2"-terpyridine	0.75 mL acetonitrile 2.25 mL water 1.74 mL 0.1M HCl
4	0.0001	2,2';6',2"-terpyridine	4.7 mL water 29 µL 6M HCl
5	0.0003	2,2'-bipyridine	2.25 mL acetonitrile 6.75 mL water

X-ray Crystallography. Single crystals from each bulk sample were isolated and mounted on MiTeGen micromounts. Data were collected on a Bruker D8 Quest equipped with a Photon II detector, using a Mo Kα source. Reflection data were collected using 0.5°ω and φ scans at 100(2) K. The APEX III software suite[29,30] was used for integrating reflection data and performing absorption corrections, which incorporates both SAINT[31] and SADABS.[32] Structure solutions (obtained using intrinsic phasing) and refinement were performed using the ShelXT package[33] and ShelXL[34] in APEX III.[31] All non-hydrogen atoms were located using Fourier difference maps and refined anisotropically. Hydrogen atoms were placed in ideal locations using HFIX33 for methyl groups, and HFIX43 for aromatic hydrogen atoms, allowing hydrogen atoms to ride on their parent atoms. All figures were prepared with Crystal Maker 8.2.2.[35] Data collection and refinement details for **1–5** are included in Table 2 and thermal ellipsoid plots for each structure are included in the SI (Figure S1-S5).

Compound **2** contains a high amount of residual electron density that persisted across a number of different crystals and collections. All attempts to determine the space group confirmed it to be P-1 and no signs of twinning were detected. Despite this, there remains disorder in the structure that could not be modelled without the use of a number of constraints and restraints. Details of the refinement are included in the cif (CCDC: 2310853).

Table 2. Crystallographic Refinement Details for Compounds 1−5.[a]

	1	**2**	**3**
CCDC no.	2310852	2310853	2310854
Formula	$[(UO_2)_3Cd_2(H_2O)_3(C_{12}H_8N_2)_2(C_7H_2NO_5)_3] \cdot 3H_2O \cdot 0.5(C_2H_3N)$	$[Cd(C_{15}H_{11}N_3)][C_{15}H_{11}N_5][(UO_2)_6Cd_2(H_2O)_2(C_{15}H_{11}N_3)_3(C_7H_2NO_5)_6] \cdot 5H_2O$	$[Cd(C_{15}H_{11}N_3)_2][(UO_2)_2(H_2O)(C_7H_3NO_5)_3] \cdot H_2O$
Formula weight	4016.05	8005.84	1720.17
Crystal System	Triclinic	Triclinic	Monoclinic
Space Group	P-1	P-1	$P2_1/n$
a, Å	11.0866(8)	18.3165(11)	10.3340(7)
b, Å	15.5084(13)	20.5702(12)	18.0600(12)
c, Å	16.4279(13)	20.6290(12)	29.042(2)
α, °	82.565(3)	61.122(2)	90
β, °	80.595(3)	64.543(2)	100.012(2)
γ, °	73.991(3)	87.934(2)	90
Volume, Å^3	2667.9(4)	5998.8(6)	2705.2(2)
Z	1	1	4
ρ_{calc}, g cm^{-3}	2.498	2.216	2.141
μ, mm^{-1}	9.764	8.596	6.541
Radiation	0.71073	0.71073	0.71073
Temp., K	100	100	100
residuals:[a] R; R_w	0.0294, 0.0577	0.0512, 0.1207	0.0236, 0.0543
Goodness of fit	1.038	1.037	1.036
	4	**5**	
CCDC no.	2310855	2310856	
Formula	$[(UO_2)Cd(C_{15}H_{11}N_3)(C_7H_3NO_5)_2]$	$[(UO_2)_2Cd(C_{10}H_8N_2)(C_7H_2NO_5)_2]$	
Formula weight	977.92	1325.03	
Crystal System	Monoclinic	Tetragonal	
Space Group	C2/c	P-4b2	
a, Å	18.9346(10)	16.4219(7)	
b, Å	13.8938(10)	16.4219(7)	
c, Å	10.6515(6)	12.9243(8)	
α, °	90	90	
β, °	94.439(3)	90	
γ, °	90	90	
Volume, Å^3	2793.7(3)	3485.4(4)	
Z	4	4	
ρ_{calc}, g cm^{-3}	2.325	2.525	
μ, mm^{-1}	6.631	9.957	
Radiation	0.71073	0.71073	
Temp., K	100	100	
residuals:[a] R; R_w	0.0235, 0.0546	0.0143, 0.0334	
Goodness of fit	1.052	1.038	

Powder X-Ray Diffraction. Powder X-Ray Diffraction (PXRD) data on the bulk reaction products of compounds **1-5** (Figure S6-S10) were used to assess the purity of the preparations. All data were collected on a Rigaku Miniflex (Cu Kα, 2θ = 3-60°) and were analyzed using the Match! software program.[36] Compounds **1, 4** and **5** resulted in pure phases. Compounds **2** and **3** were

impure. Attempts to match the unknown phases to known compounds were unsuccessful and as such remain unidentified.

Optical Measurements. Steady-state luminescence scans of **1-5** were collected at 298K with a Fluorolog-3 photoluminescence spectrophotometer from Horiba using a 450 W xenon arc lamp combined with a double excitation monochromator and double emission monochromator. A photomultiplier tube at 950 V was used as the emission detector. Crystalline samples (purity confirmed by PXRD or by SCXRD where there was no bulk purity and single crystals were used for analysis) were mounted on a quartz plate using non-emitting high vacuum grease. Raman spectra of **1-5** were collected on single crystals using a HORIBA LabRAM HR Evolution Raman Microscope over the 50–2000 cm^{-1} range. An excitation line at 785 nm was used for each collection.

Computational details.

Natural Bond Orbitals (NBO)[37]*, Quantum Theory of Atoms in Molecules (QTAIM)*[38]. The uranyl-cation interactions between the UO_2^{2+} and Cd^{2+} units in **1-5** were investigated and quantified via Density Functional Theory as implemented in Gaussian 16.[39] Single point energy calculations were performed on models constructed directly from unoptimized crystallographic fragments consisting of the closest Cd-oxo interaction and all ligands coordinated to the Cd^{+} and UO_2^{2+} units. In compounds **1** and **2,** which contained more than one uranyl with a closely interacting Cd^{2+}, separate models were made for each of the close interactions. The B3LYP[40,41] functional, which has been shown to reproduce experimental parameters of uranyl complexes with high accuracy, was used for all calculations.[42,43] The 6-311g(d,p) basis set and associated pseudopotential was used for all H, C, N, and O atoms.[44] The modified scalar-relativistic effective core potential (ECP) basis set DEF2TZVP[45,46] and associated pseudopotential was used for Cd atoms. The ECP60MWB and ECP60MWB_SEG valence basis set was used for all U atoms.[47–49] No additional corrections were used for the energy calculations and a tight convergence criterion was used. Second order perturbation theory (SOPT) was applied to (i) quantify the magnitude of the interaction (in kcal/mol) between the donor and acceptor and (ii) identify particular natural bonding orbitals involved. Quantum theory of atoms in molecules[49] (QTAIM) analysis of bonding properties at the bond critical points (BCPs) was performed in the AIMA11 software suite[50] using the DFT converged wavefunction. Models generated and used for NBO and AIMA11 calculations can be found in the SI (Figure S11) along with a sample input file (Sample S1).

Buried Volume. Percent buried volume calculations were performed using SambVca 2.1.[51] The oxo group was designated as the center of the sphere with the uranium atom as the only coordinating ligand. The radius used for the calculation was the Bondi Radius scaled by 1.17 as is the default with a sphere radius of 3.5. Hydrogen atoms were included in the calculation.

Results and Discussion

Structural Descriptions.

Compound **1**, $[(UO_2)_3Cd_2(H_2O)_3(phen)_2(chel)_3] \cdot 3H_2O \cdot 0.5$(acetonitrile), crystallizes in the space group *P-1*. The asymmetric unit contains three crystallographically unique UO_2^{2+} cations (Figure 1). All three adopt a pentagonal bipyramidal geometry with one tridentate chelidamate ligand and two monodentate chelidamate ligands coordinated in the equatorial plane. All chelidamate ligands are fully deprotonated with an overall -3 charge. The axial U=O bonds have lengths of: U1 - 1.781(4) Å (O1) and 1.799(4) Å (O2), U2 – 1.790(4) Å (O3) and 1.768(5) Å (O4), U3 – 1.774(4) Å (O5) and 1.779(4) Å (O6). The uranyl cations have ∠O-U-O of 176.61(18)° (U1), 176.6(2)° (U2), and 175.6(2)° (U3). The asymmetric unit also contains two crystallographically unique six-coordinate Cd^{2+} centers. Cd1 is coordinated by a bidentate phenanthroline ligand and three water molecules and interacts closely with the oxo group of U1 (O2) at a distance of 2.367(4) Å. Cd2 is coordinated by two bidentate phenanthroline ligands and by two symmetrically equivalent uranyl oxo groups (O3) at a distance of 2.330(4) Å. The angles ∠U-O-Cd of these Cd-oxo interactions are 153.7(2)° (Cd1) and 144.7(2)° (Cd2). In the lattice are three water molecules and one partially occupied acetonitrile molecule. Packing of **1** (Figure 2) features 2-dimensional sheets consisting of interconnected UO_2^{2+} and chelidamate ligands. These sheets are assembled into a 3-dimensional network via the Cd-oxo interactions of Cd2 with O3. The structure also exhibits π-stacking between adjacent phenanthroline and chelidamate ligands, as well as hydrogen bonding between water molecules in the lattice and the chelidamate ligand oxygen atoms and the water molecules coordinated to Cd1.

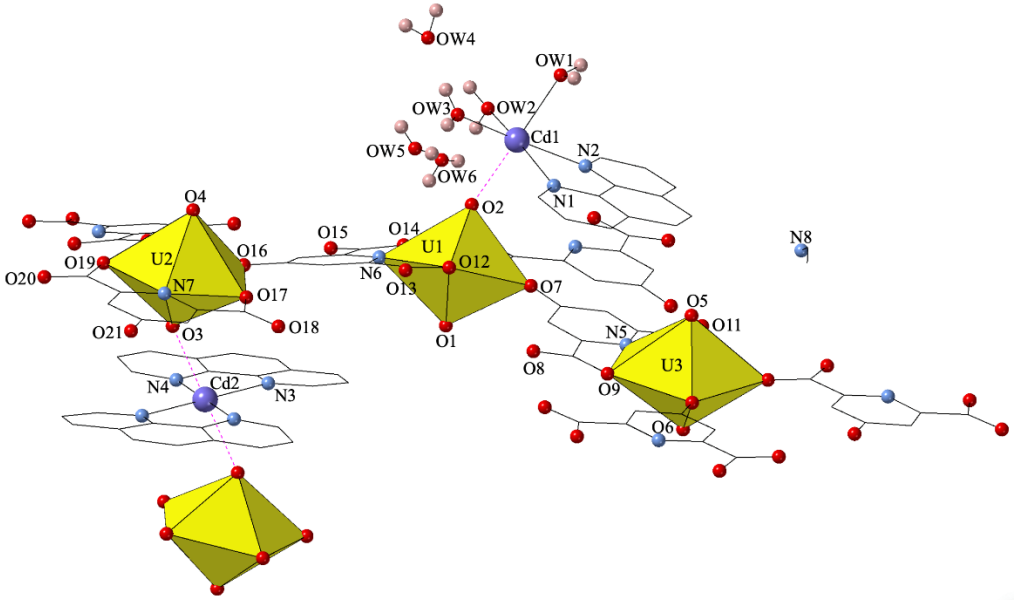

Figure 1. Local representation of compound **1** detailing the metal coordination environments. Uranyl polyhedra are shown in yellow; Cd, N, and O are lilac, blue, and red spheres respectively.

Cd-oxo interactions are depicted by dotted pink lines. H atoms on organic ligands have been omitted for clarity.

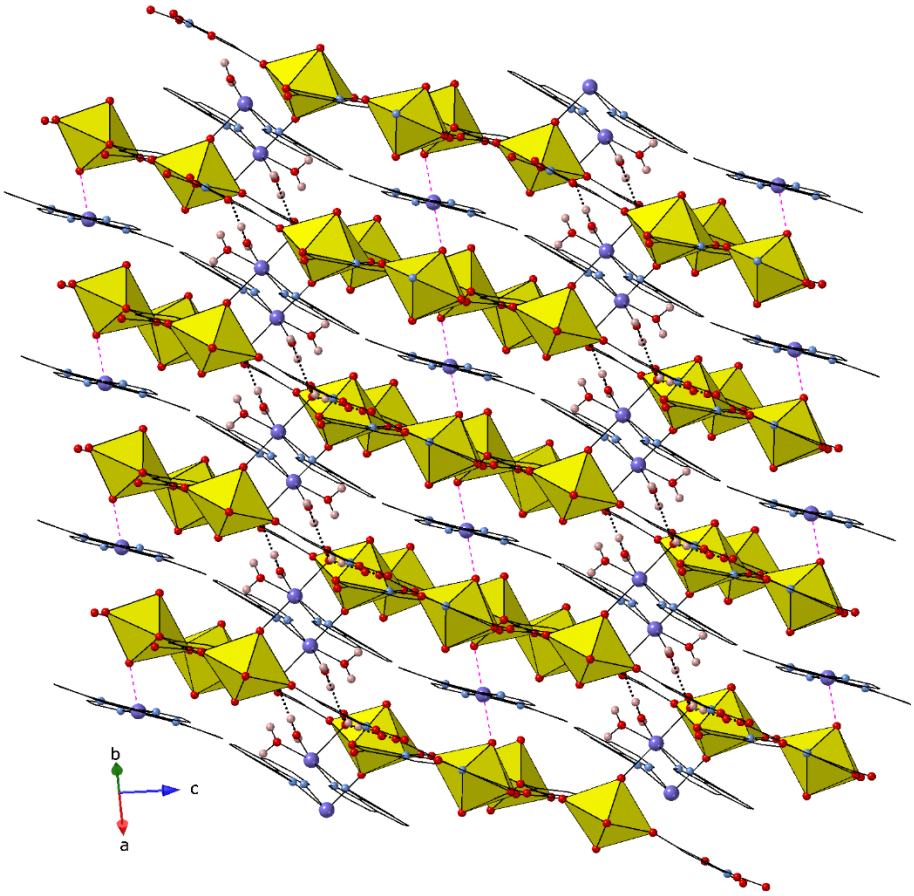

Figure 2. Global structure of **1** shown along [100]. π-stacking is depicted with blue dotted lines and H-bond interactions are depicted with grey dotted lines. Cd-oxo interactions are depicted by dotted pink lines. Solvent acetonitrile molecules have been omitted for clarity.

Compound **2**, $[Cd(terpy)][H_2terpy][(UO_2)_6Cd_2(H_2O)_2(terpy)_3(chel)_6] \bullet 5H_2O$, crystallizes in the space group *P-1*. The asymmetric unit features six crystallographically unique UO_2^{2+} cations (Figure 3). All six adopt a pentagonal bipyramidal geometry with one tri-dentate chelidamate ligand and two monodentate chelidamate ligands coordinated in the equatorial plane. All chelidamate ligands are fully deprotonated with an overall -3 charge. The axial U=O bonds have bond lengths of: U1 - 1.797(7) Å (O1) and 1.782(7) Å (O3), U2 – 1.780(8) Å (O4) and 1.782(8) Å (O5), U3 – 1.775(8) Å (O6) and 1.797(7) Å (O7), U4 - 1.785(8) Å (O8) and 1.766(8) Å (O9), U5 – 1.775(8) Å (O10) and 1.779(7) Å (O11), U6 – 1.757(9) Å (O12) and 1.777(9) Å (O13). The uranyl cations have ∠O-U-O of 178.4(3)° (U1), 177.9(3)° (U2), 178.5(3)° (U3), 179.4(4)° (U4), 177.1(4)° (U5), and 176.8(5)° (U6). The asymmetric unit also features two crystallographically unique Cd^{2+} cations. Cd1 is six-coordinate and is coordinated by one tridentate terpyridine ligand and two water molecules. It interacts closely with the oxo group of U1 (O1) at a distance of 2.460(7) Å. Cd2 is seven-coordinate and is coordinated by two tridentate terpyridine ligands. It

interacts closely with the oxo group of U3 (O7) at a distance of 2.550(7) Å. The ∠U-O-Cd of the Cd-oxo interactions are 174.1(4)° (Cd1) and 170.6(4)° (Cd2). There is also a partially occupied Cd^{2+}/terpyridine moiety and a partially occupied doubly protonated terpyridine molecule in the lattice. There are five partially occupied water molecules that assemble via hydrogen bonding. Packing of **2** (Figure 4) features 2-dimensional sheets of UO_2^{2+} liked by chelidamate ligands. The structure exhibits π-stacking between adjacent terpyridine and chelidamate ligands, as well as hydrogen bonding between water molecules in the lattice and the chelidamate ligand oxygen atoms and the water molecules coordinated to Cd1.

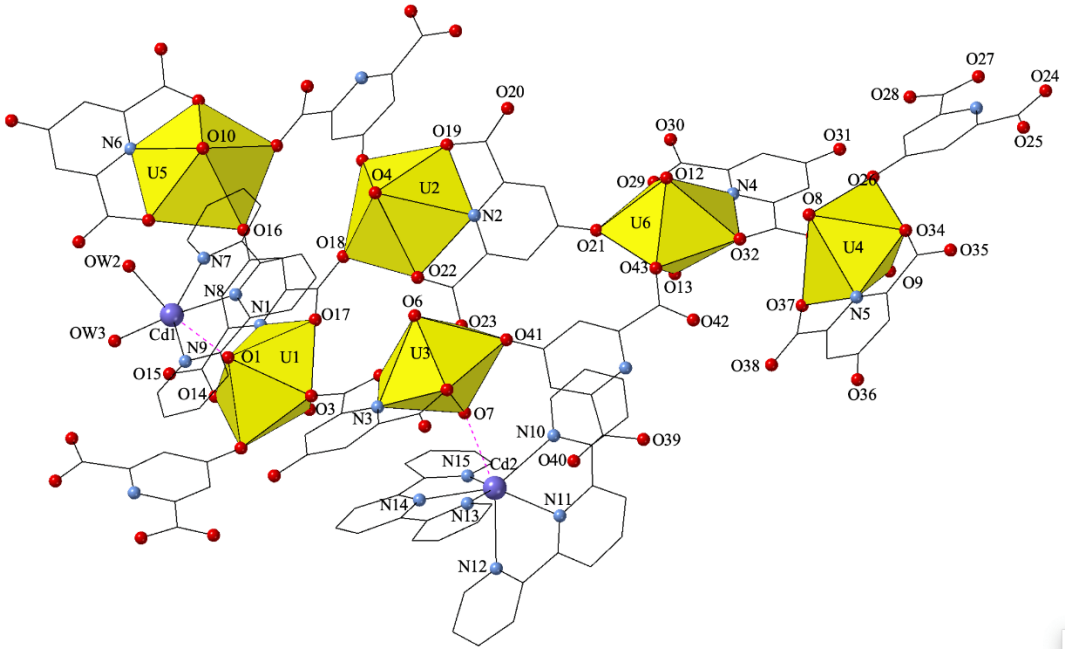

Figure 3. Local representation of compound **2** detailing the metal coordination environments. Cd-oxo interactions are depicted by dotted pink lines. Lattice molecules (Cd^{2+}/terpy, H_2terpy^{2+}, and water) are omitted for clarity.

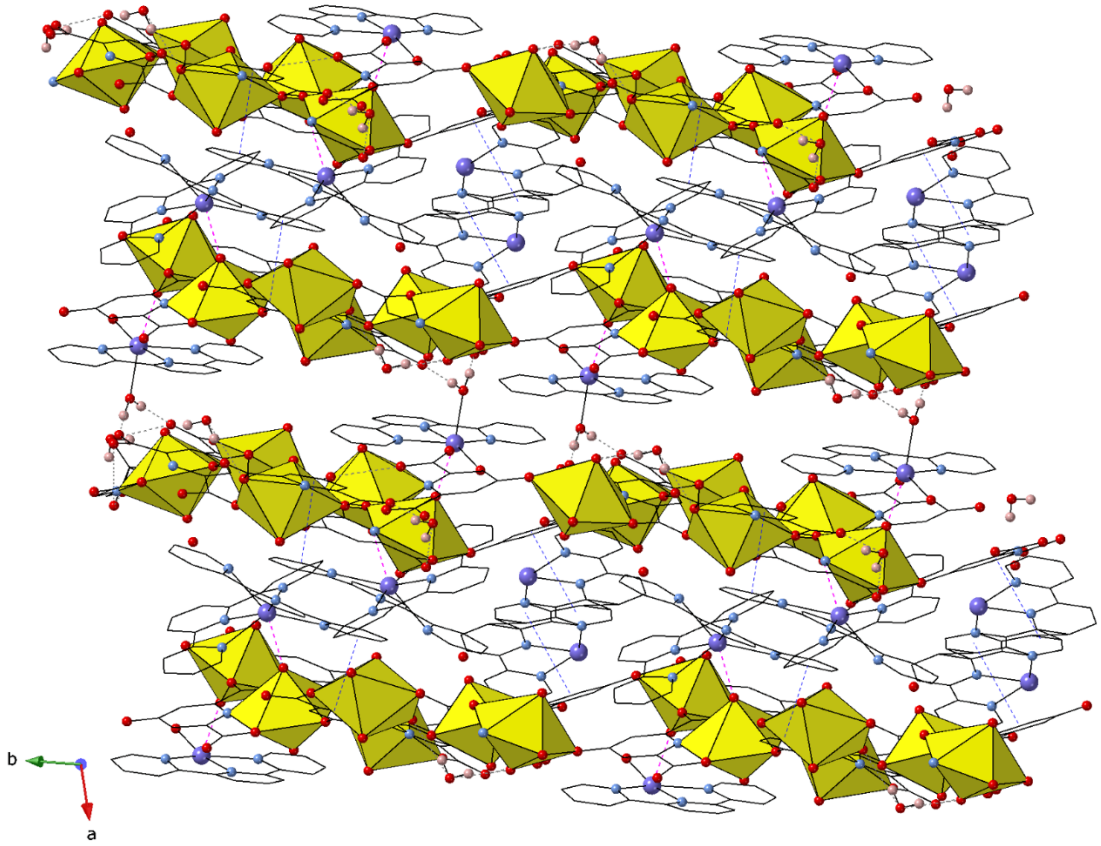

Figure 4. Global structure of compound **2** shown along the *c*-axis. π-stacking is depicted with blue dotted lines and H-bond interactions are depicted with grey dotted lines. Cd-oxo interactions are depicted by dotted pink lines.

Compound **3**, $[Cd(terpy)_2][(UO_2)_2(H_2O)(Hchel)_3] \cdot H_2O$, crystallizes in the space group *P2₁/n*. The asymmetric unit contains two crystallographically unique UO_2^{2+} cations (Figure 5). U1 adopts a pentagonal bipyramidal geometry with one tridentate chelidamate ligand, one monodentate chelidamate ligand, and one water molecule coordinated in the equatorial plane. U2 adopts a hexagonal bipyramidal geometry with two tridentate chelidamate ligands coordinated in the equatorial plane. All chelidamate ligands feature a protonated hydroxy group and have an overall charge of -2. The axial U=O bonds have bond lengths of: U1 - 1.772(2) Å (O3) and 1.769(2) Å (O4), U2 – 1.765(2) Å (O1) and 1.778(2) Å (O2). The uranyl cations have ∠O-U-O of 178.59(10)° (U1) and 177.44(10)° (U2). The asymmetric unit contains one crystallographically unique six-coordinate Cd^{2+} cation. Cd1 is coordinated by two tridentate terpyridine ligands. The closest uranyl oxo group to Cd1 is O2 at a distance of 4.294(2) Å and ∠U-O-Cd of 143.17(9)°. In the lattice, there two water molecules. Packing of **3** (Figure 6) features dimeric units composed of UO_2^{2+} (U1 and U2) and chelidamate ligands, and monomeric units composed of Cd^{2+} and terpyridine. These units are connected via π-stacking interactions between adjacent chelidamate and terpyridine ligands. Adjacent uranyl/chelidamate dimers are connected via a hydrogen bonding network between adjacent chelidamate ligands and lattice water molecules.

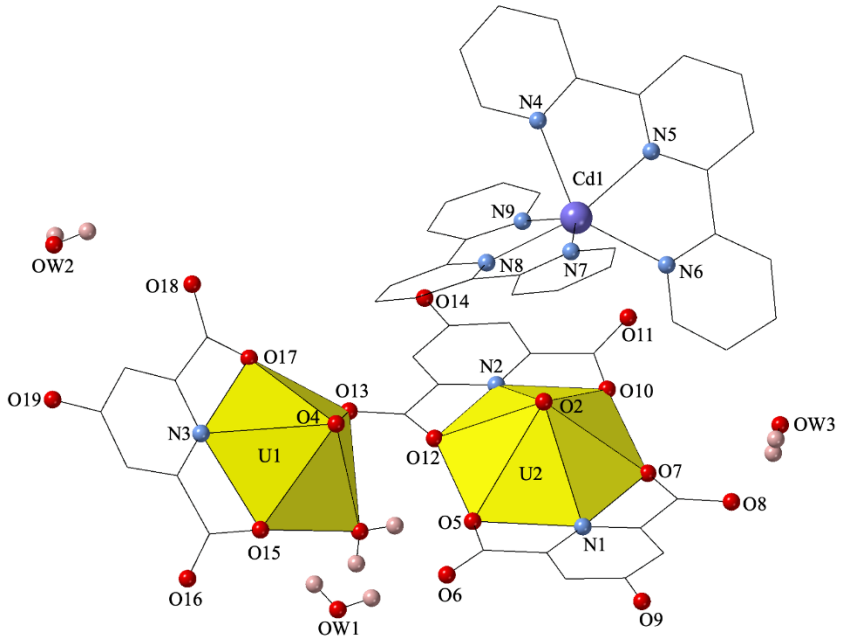

Figure 5. Local representation of compound **3** detailing metal coordination environments.

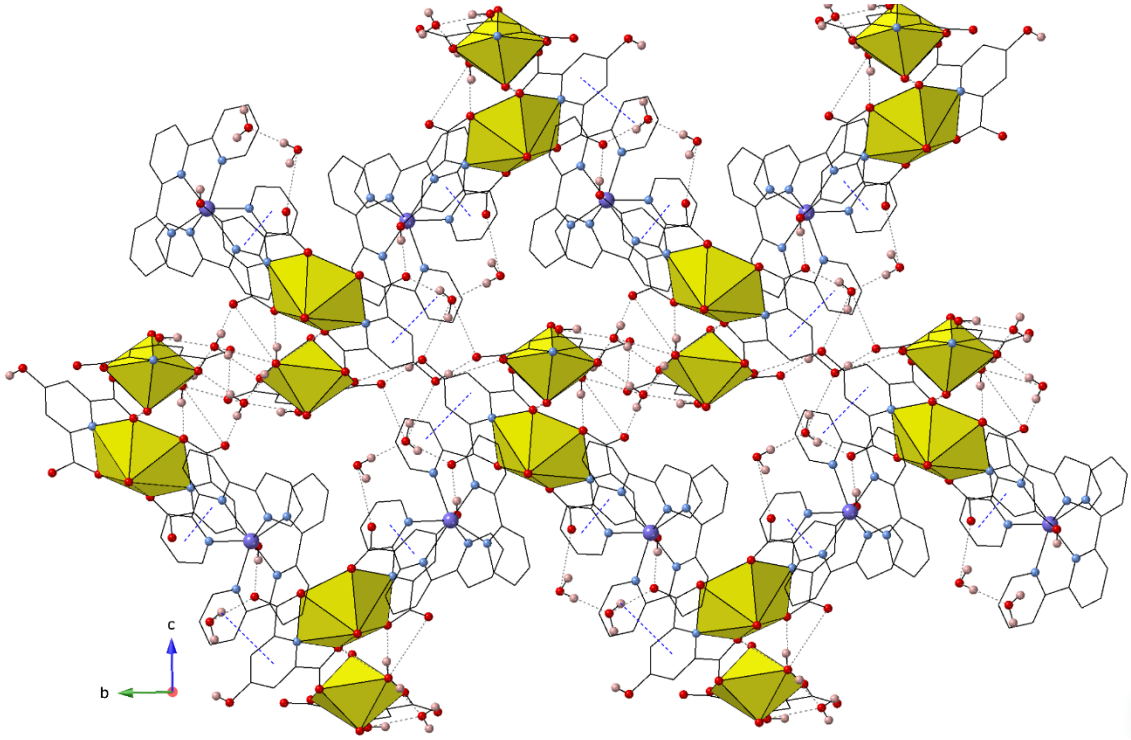

Figure 6. Global structure of compound **3** shown along the *a*-axis. π-stacking is depicted with blue dotted lines and H-bond interactions are depicted with grey dotted lines.

Compound **4**, $[(UO_2)Cd(terpy)(Hchel)_2]$, crystallizes in the space group *C2/c*. The asymmetric unit contains one crystallographically unique UO_2^{2+} cation (Figure 7). U1 adopts a hexagonal bipyramidal geometry with two tridentate chelidamate ligands coordinated in the

equatorial plane. Both chelidamate ligands feature a protonated hydroxy group and have an overall charge of -2. The axial U=O bonds are symmetrically equivalent and have a bond length of 1.764(2) Å. The ∠O-U-O is 180.0°. The asymmetric unit contains one crystallographically unique seven-coordinate Cd^{2+} cation. Cd1 is coordinated by one tridentate terpyridine ligand and two bidentate chelidamate ligands. The closest uranyl oxo group to Cd1 is O1 at a distance of 4.901(2) Å and ∠U-O-Cd of 67.48(6)°. Packing of **4** (Figure 8) features 1-dimensional UO_2^{2+} and chelidamate ligand chains that run along the a-axis. These chains are connected via π-stacking interactions between adjacent terpyridine ligands and H-bond interactions between adjacent chelidamate ligands.

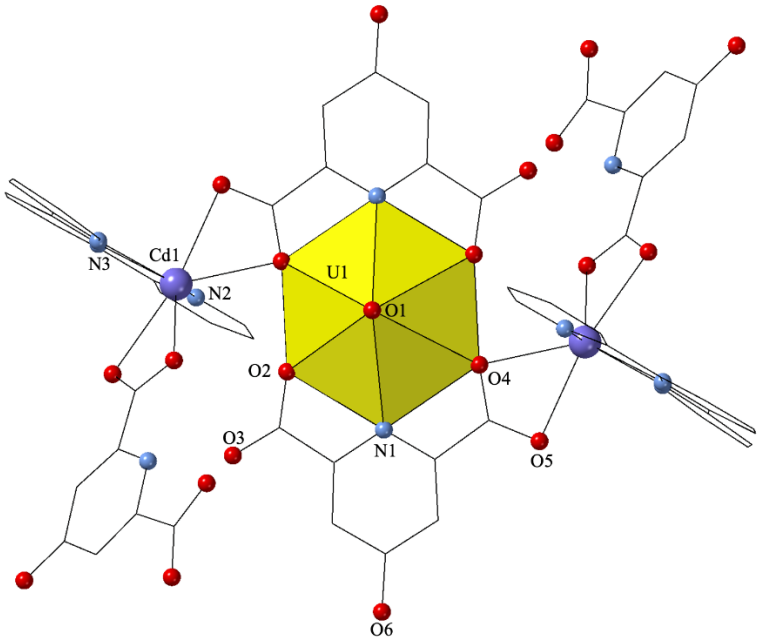

Figure 7. Local representation of compound **4** detailing the metal coordination environments.

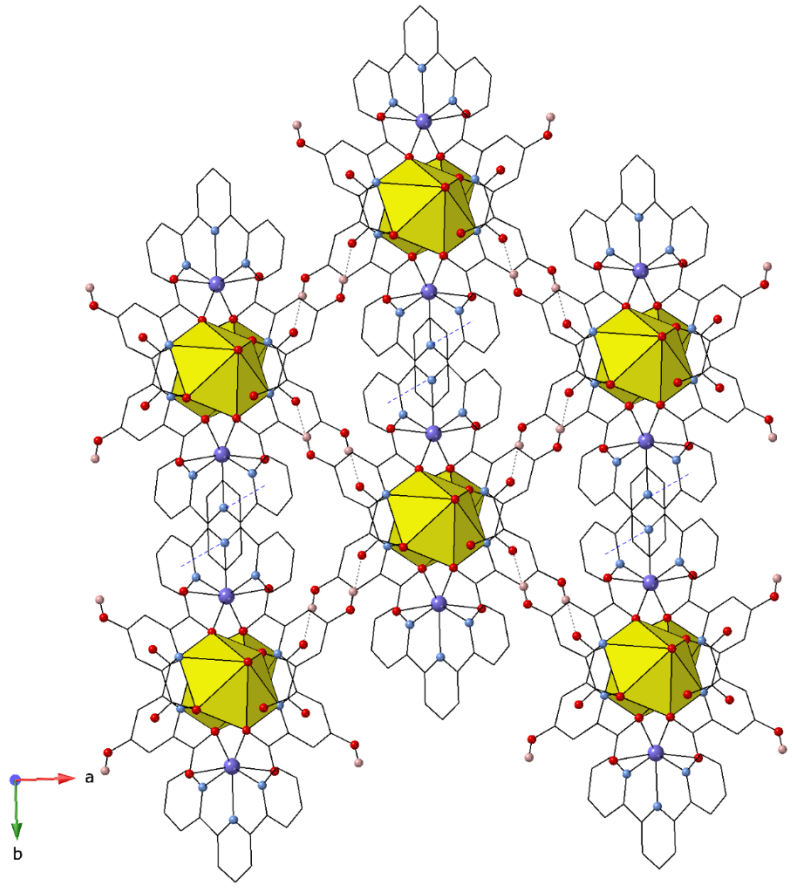

Figure 8. Global structure of compound **4** shown along the *c*-axis. π-stacking is depicted with blue dotted lines and H-bond interactions are depicted with grey dotted lines.

Compound **5**, $[(UO_2)_2Cd(bipy)(chel)_2]$, crystallizes in the space group *P-4b2*. The asymmetric unit contains one crystallographically unique UO_2^{2+} cation (Figure 9). U1 adopts a pentagonal bipyramidal geometry with one tridentate chelidamate ligand, and two monodentate chelidamate ligands. All chelidamate ligands are fully deprotonated with an overall -3 charge. The axial U=O bonds have bond lengths of: 1.778(3) Å (O1) and 1.769(3) Å (O2). ∠O-U-O is 178.05(15)°. The asymmetric unit contains one crystallographically unique six-coordinate Cd^{2+} cation. Cd1 is coordinated by two bidentate bipyridine ligands and bridges to the uranyl center via two monodentate chelidamate ligands. The closest uranyl oxo group to Cd1 is O2 at a distance of 5.219(3) Å and ∠U-O-Cd of 78.65(11)°. Compound **5** (Figure 10) features a 3-dimensional network linked by chelidamate ligands bridging between uranyl cations and cadmium (II) cations. This network displays π-stacking between adjacent terpyridine and chelidamate ligands.

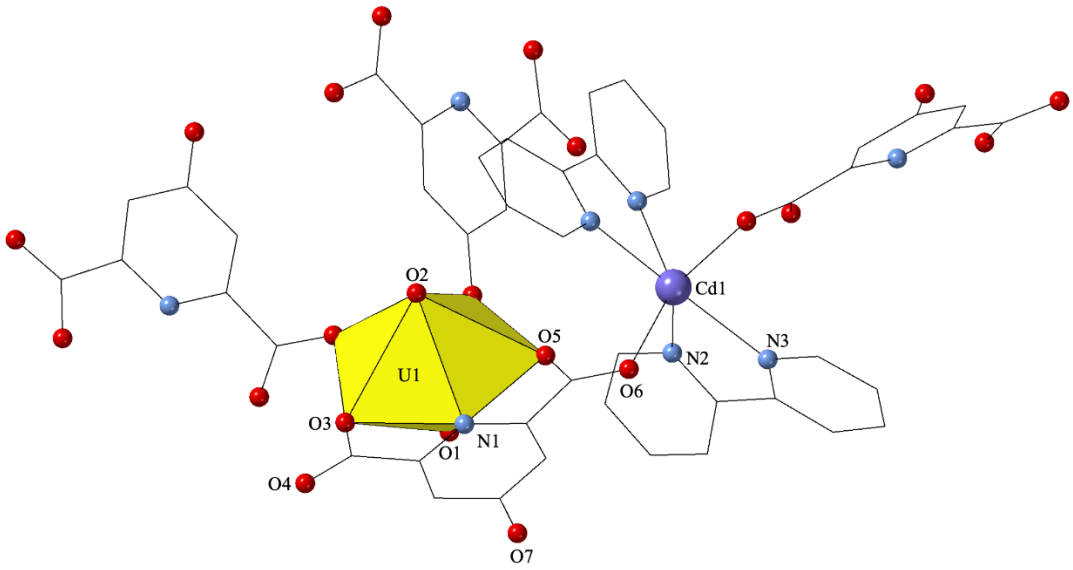

Figure 9. Local representation of compound **5** detailing the metal coordination environments.

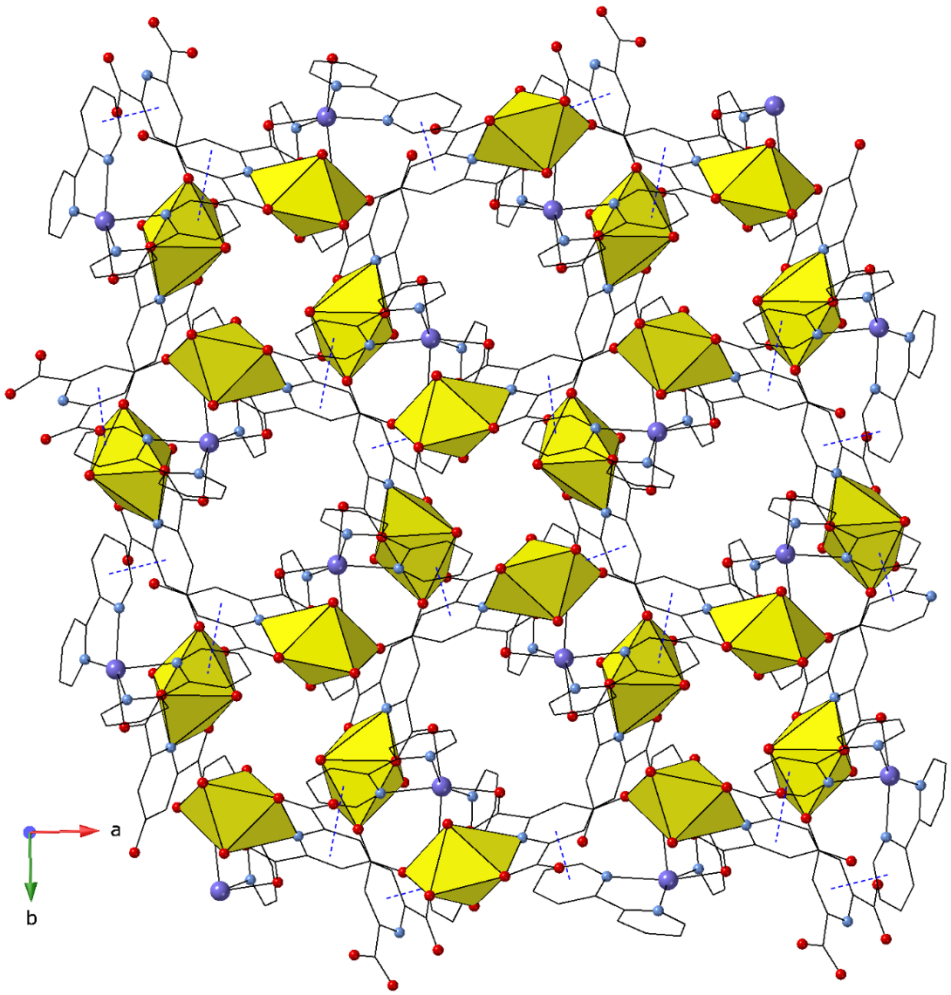

Figure 10. Global structure of compound **5** shown along the *c*-axis. π-stacking is depicted by blue dotted lines.

Cd^{2+} Interactions with Uranyl Oxo atoms. In our previous work uranyl-oxo interactions with Pb^{2+} and Ag^{+}, [26,27] we determined that crystallographic M^{n+}-oxo distances served as good indication of the strength of the interaction: shorter distances indicated stronger interactions. When comparing interaction effects between the two different metals, the effects of Pb^{2+} cations were much stronger than those of Ag^{+} cations at comparable distances. We attributed this to the lower polarizability of Pb^{2+} as compared to Ag^{+}. We now expand our efforts to the even less polarizable Cd^{2+} cation to probe further the nature of these effects.. The structural data shows two compounds (**1** and **2**) that display short Cd-oxo contacts and three (**3-5**) that do not. Compounds **1** and **2** each feature multiple unique uranyl centers, two of which (in each) display very close Cd^{2+}-oxo contacts. In Table 3, we report both of these close contacts for **1** and **2**, and the closest distances for **3-5**. These compounds display a range of values from 2.330(4) Å to 5.219(3) Å which all fall within the range of Cd-oxo distances reported in the CSD.[28]

The interaction of van der Waals spheres of two atoms A and B, denoted as %vdW (where $\%vdW = \frac{d_{A-B}}{r_{vdW,A}+r_{vdW,B}} * 100\%$), gives a structural metric to quantify the strength of an interaction and allows for comparison between metal cations of different sizes. We employ this for our compounds (Cd radius: 1.53 Å and O radius: 1.52 Å),[52] to classify Cd-oxo interactions as significant (%vdW < 100) and weak or no interaction (%vdW > 100). [52] The Cd-O %vdW are reported in Table 3 and range from 76% to 171%. The values reported for compounds **1** and **2** all fall well within 100% of the van der Waals radii, whereas those in compounds **3-5** all fall outside.

Close interaction of a metal cation with the uranyl oxo group can lead to U=O bond asymmetry as reported by Arnold et al. In extreme cases, this can even lead to the reduction of U(VI) to U(V).[21–23] In compounds **1** and **2**, we see significant lengthening of the U=O bond that interacts closely with a Cd^{2+} cation as compared to its non-interacting counterpart. The asymmetry of these bonds varies from 0.015 Å (Compound **2(U1)**) to 0.022 Å (Compounds **1(U2)** and **2(U3)**). These values do not seem to correlate exactly with the distance of the M^{n+}-oxo interaction but we note that the bond asymmetry is more pronounced in these compounds than what observed previously with Ag^{+} and Pb^{2+}.[26,27] Significant bond asymmetry was only reported in one of the Pb^{2+} containing complexes which interacted at a distance of 81 %vdW (with a bond difference of 0.02 Å). Other Pb^{2+}/UO_2^{2+} compounds, even when interacting at similar %vdW to the Cd^{2+}/UO_2^{2+} compounds did not display this asymmetry, and none of the Ag^{+}/UO_2^{2+} compounds displayed significant asymmetry even at closer interaction distances of 76 %vdW. As Cd^{2+} is less polarizable than Pb^{2+} and significantly less polarizable than Ag^{+}, these results support Arnold et. al.'s observations and our previous conclusions that harder metals promote greater uranyl bond asymmetry.[21–23]

Table 3. Summary of crystallographically determined Cd-oxo interaction parameters.

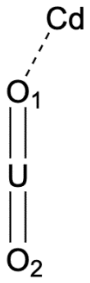

Compound	Cd···O1 (Å)	%vdW	U=O1 (Å)	U=O2 (Å)	Cd···O1=U (°)
1 (U1)	2.367(4)	78%	1.799(4)	1.781(4)	153.7(2)
1 (U2)	2.330(4)	76%	1.790(4)	1.768(5)	144.7(2)
2 (U1)	2.460(7)	81%	1.797(7)	1.782(7)	174.1(4)
2 (U3)	2.550(7)	84%	1.797(7)	1.775(8)	170.6(4)
3	4.294(2)	141%	1.778(2)	1.765(2)	143.17(9)
4	4.901(2)	161%	1.764(2)	1.764(2)	67.48(6)
5	5.219(3)	171%	1.769(3)	1.778(3)	78.65(11)

Spectroscopic Properties.

Previous work has shown that interactions with the uranyl cation, both in the equatorial coordination plane and with the axial oxo groups will affect the spectroscopic properties of the uranyl cation.[9,17,18,21,22,43,53,54] Our work with Pb^{2+} and Ag^{+} has demonstrated that close interactions of these metals with the uranyl oxo group leads to decreased luminescence intensity and red-shifting of the Raman active U=O symmetric stretch.[26,27] Here, we apply that same metric to Cd^{2+}/UO_2^{2+} compounds to prove the changes in the U=O bonds.

Luminescence Spectroscopy. Uranyl-containing compounds typically display bright green luminescence corresponding to the emission band which ranges from 470 nm to 650 nm and can have up to six vibrationally resolved peaks. The emission profile occurs due to an electronic transition between uranium 5f δ_u and ϕ_u orbitals and the ground state uranyl bonding orbitals ($3\sigma_u$, $3\sigma_g$, $1\pi_g$, $2\pi_u$) and vibronic coupling with the 855 cm^{-1} U=O symmetric stretch.[3] The excitation profile for the uranyl-containing compounds features two bands centered around 420 nm and 340 nm corresponding to the axial and equatorial LMCT transitions respectively.[8]

The emission and excitation profiles for compounds **1-5** are shown in Figure 11. The intensities of the emission of compounds **1** and **2** are significantly lower than those of compounds **3-5**. As a result of this decreased intensity, the resolution of compounds **1** and **2** is poor, resulting in loss of the clearly defined vibrationally resolved peaks in the emission and the two clearly defined bands in the excitation. Compounds **3-5** all display the clearly defined peaks in the emission and **3** and **4** display two clearly separate bands in the excitation as is typical for uranyl-containing compounds. It is worth noting that both compounds **1** and **2** contain multiple unique

uranyl centers, some that do have close interactions and others that are not directly interacting with a Cd^{2+} cation. Despite this, we still see decreased emission as a whole. We suspect that the weaker emission signal we see in these compounds is a result of the uranyl centers that are *not* closely interacting with a Cd^{2+} cation and therefore remain unperturbed. The overall intensity is decreased as a result of the loss of intensity in the centers where Cd^{2+} *is* interacting closely.

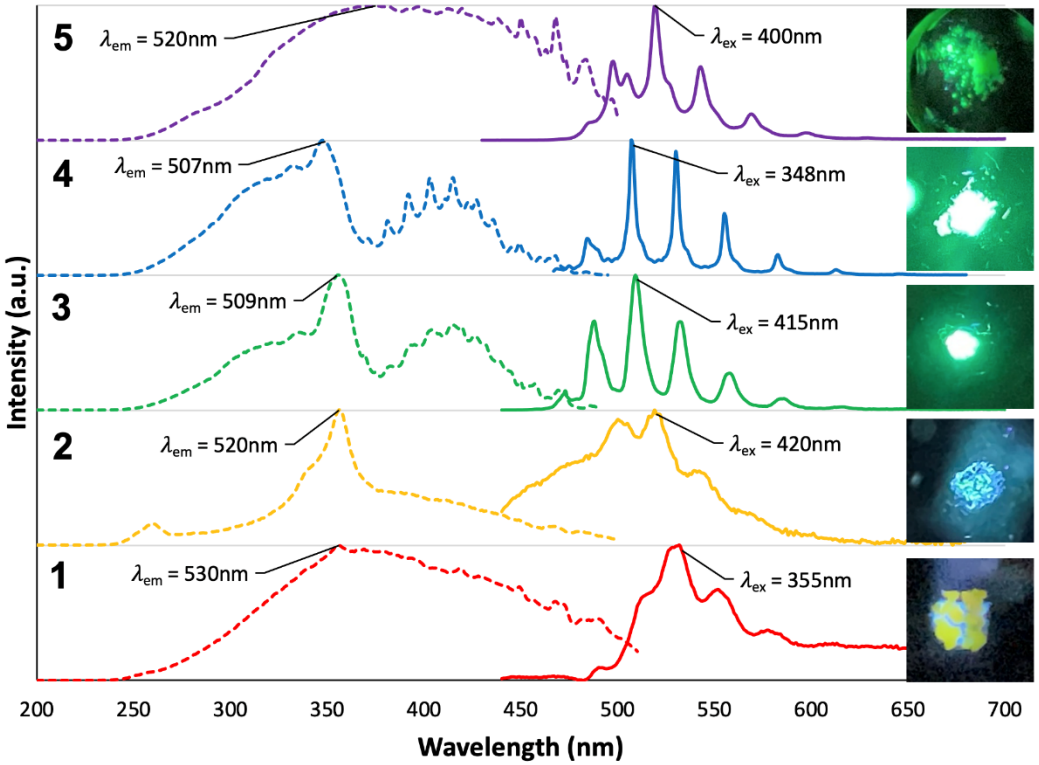

Figure 11. Luminescence spectra of compounds **1-5** at 298K with images under a 340 nm UV light.

These results only allow for qualitative comparison between these compounds, yet a relationship between metal polarizability and the loss of luminescence intensity can still be inferred. The loss of luminescence intensity displayed in **1** and **2**, where the %vdW contacts all fall below 85%, is similar to the loss of intensity displayed in the Pb^{2+}/UO_2^{2+} compounds with close contacts (87 %vdW or lower). These results contrast with what was observed in the softer Ag^{+} cations which did not consistently decrease the emission intensity.[27]

Raman spectroscopy. We turn to Raman spectroscopy for a more quantitative and sensitive spectroscopic probe of the effects of these M^{n+}-oxo interactions on U=O bond strength. [3,17,43,54] The uranyl cation has three vibrational modes: the symmetric stretch (ν_1, Raman active), the asymmetric bend (ν_2, IR active), and the asymmetric stretch (ν_3, IR active). Of these, the Raman active symmetric stretch is easily identifiable and is sensitive to interactions with the uranyl cation both in the equatorial plane and with the axial oxo groups. Both of these types of interactions tend to cause red-shifting of the U=O symmetric stretch peak as a result of weakening of the U=O bond.

The U=O symmetric stretch is typically observed in the 860-880 cm^{-1} region but has been reported across the range of 750 to 900 cm^{-1}.[53]

The Raman spectra for compounds **1-5** are presented in Figure 12. Assignment of the U=O symmetric stretch is straightforward in **4** and **5** as there is only one unique uranyl center in each compound; 856 cm^{-1} for compound **4** and 847 cm^{-1} for compound **5**. In compounds **1-3** however, assignment of the U=O symmetric stretches is a little more difficult as there are multiple unique uranyl centers that each have different bond strengths and therefore different stretching frequencies. For compound **3**, which has *two* symmetrically unique uranyl centers, we can assign these as corresponding to the 844 and 851 cm^{-1} peaks in this region. Compound **2** contains *six* unique uranyl centers. Of these centers, two feature close Cd-oxo contacts and four do not. We see a number of features in the 790 to 850 cm^{-1} region. While it is only possible to clearly identify two peaks, there are a number of shoulders that occur likely due to overlap of similar energy uranyl stretches. Knowing this, and keeping in mind the longer U=O bonds seen in the structural data corresponding to the U=O bonds possessing closer Cd-oxo contacts, we tentatively assign the feature at 802 cm^{-1} as belonging to one of the uranyl bonds possessing a close Cd-oxo contact. We expect the other to appear in the same region and it may explain the shoulder that can be seen around 797 cm^{-1}. In the structural data, uranyl centers not interacting closely with the Cd^{2+} cations, have shorter bond lengths that would correspond to higher energy peaks. We tentatively assign the 839 cm^{-1} peak to one of these centers while we would expect the other non-interacting centers to correspond to the shoulders at 829 cm^{-1}, 834 cm^{-1}, and 853 cm^{-1}. These assignments are tentative as we are aware that there could be ligand-based stretches in this region as well. In compound **1**, there are three unique uranyl centers. Two display close Cd-oxo contacts and we assign these as corresponding to the 799 cm^{-1} and 807 cm^{-1} peaks as we see the lengthened bonds in the structural data. The 840 cm^{-1} peak we assign as the non-interacting uranyl center. In agreement with the significant asymmetry (as compared to the Pb^{2+}/UO_2^{2+} and the Ag^{+}/UO_2^{2+} compounds) displayed in the structural data, compounds **1** and **2** display *greater* red-shifting than observed in Pb^{2+} or Ag^{+} compounds, further confirming the greater influence of Cd^{2+} on the strength of the U=O bonds.

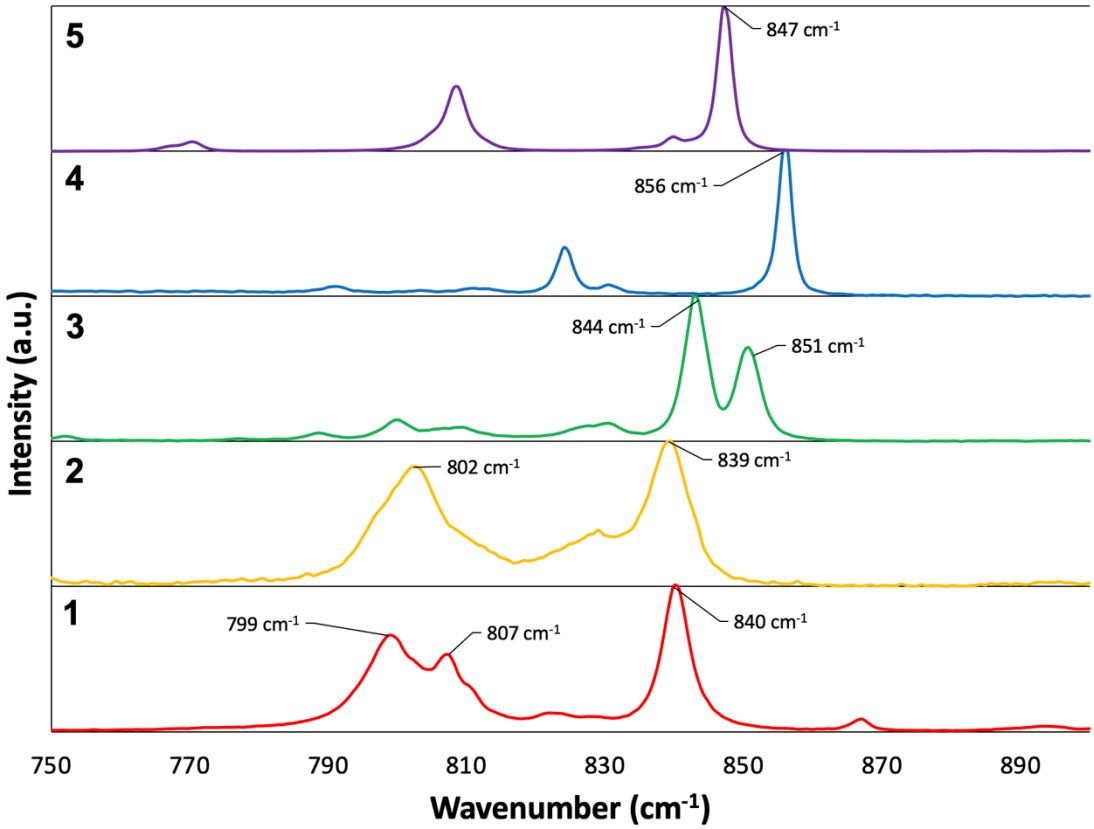

Figure 12. Raman spectra of compounds **1-5** at 298 K.

Characterizing Uranyl Second Sphere Interactions and Inner Sphere Bonding

Second Sphere Interactions. We use Natural Bond Orbital (NBO) Second Order Perturbation Theory (SOPT) to study the interactions occurring locally between the metal cations and the uranyl oxo-groups. These calculations determine orbital pairs and a stabilization energy in kcal/mol afforded to the structure as a result of interactions between these orbital pairs. This stabilization energy is calculated as a function of the orbital overlap and energy difference as described in Equation 1.

$$E(2) = \Delta E_{ij} = q_i \frac{F(i,j)^2}{\varepsilon_j - \varepsilon_i} \quad (1)$$

For the Cd-oxo interactions, SOPT determined three types of orbital interactions occurring (Figure 13): 1) Cd *d* valence orbital → UO_2 σ/π^* antibonding orbital (2) O sp^x lone pair → Cd *s* orbital, and (3) UO_2 σ/π bonding orbital → Cd *s* orbital.

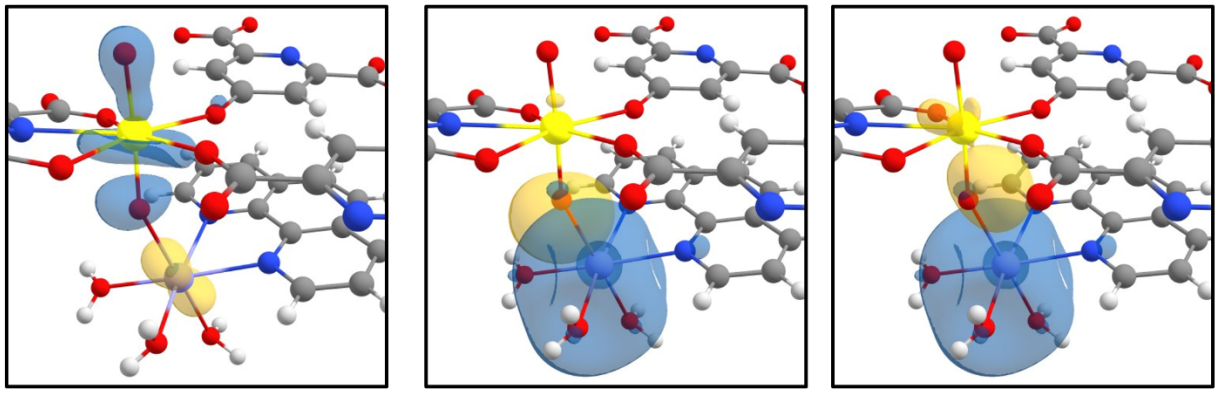

Type 1: Cd *d* → UO_2 *σ/π** Type 2: O sp^x → Cd *s* Type 3: UO_2 *σ /π* → Cd *s*

Figure 13. Isodensity renderings of representative NBOs involved in Cd-oxo interactions using compound **1(U1)** as a model.

The stabilization energy values calculated for each of these interactions are reported in Table 4. A higher energy in kcal/mol indicates a stronger interaction resulting from better overlap and energy matches in the orbitals involved. The highest stabilization energy occurs as a result of the Type 2 interaction between the O sp^x and the empty Cd *s* orbitals. The Type 1 and 3 interactions are generally similar in strength and weaker than Type 2 but are notable as they involve the bonding and antibonding orbitals of the uranyl. In Type 1, the uranyl antibonding orbital serves as an acceptor and in the Type 3 interaction, the uranyl bonding orbital serves as donor. We would expect both of these interactions to lead to weakening of the U=O bonds consistent with the significant red-shifting we see in the Raman spectra. It is of note that SOPT analysis done for the Pb^{2+}/UO_2^{2+} and Ag^{+}/UO_2^{2+} included a fourth type of interaction composed of a donor Pb *s*/Ag *d* orbital and an acceptor U *5f* orbital. Whereas this interaction was minor in those compounds, its absence in all of the Cd^{2+}/UO_2^{2+} compounds, including those with very close contacts, is noteworthy.

Table 4. Second Order Perturbation Theory calculated stabilization energies (kcal/mol) and orbitals involved in charge transfer.

		$Cd^{2+} \rightarrow UO_2^{2+}$	$UO_2^{2+} \rightarrow Cd^{2+}$		
	Cd-O Distance	**Type 1 Cd d → UO_2 σ* (kcal/mol)**	**Type 2 O sp^x → Cd s (kcal/mol)**	**Type 3 UO_2 σ → Cd s (kcal/mol)**	**Total (kcal/mol)**
1U1	2.367(4)	0.72	14.05	1.23	16.00
1U2	2.330(4)	0.67	10.85	2.10	13.62
2U1	2.460(7)	0.68	11.50	0.30	12.48
2U2	2.550(7)	0.58	11.24	0.06	11.88
3	4.294(2)	0.00	0.19	0.00	0.19
4	4.901(2)	0.00	0.05	0.00	0.05
5	5.219(3)	0.00	0.00	0.00	0.00

We have summed the stabilization energies for each of the three different types of orbital donor/acceptor pairs to determine the total stabilization energy of the interaction and have plotted them against the Cd-oxo distance (Figure 14). The stabilization energy value is higher for the compounds with closer interactions, indicating a stronger interaction as a result of approaching metal cation. The highest stabilization energy (compound **1U1**) is 16.00 kcal/mol, whereas the second highest stabilization energy corresponds to compound **1U2** despite the interaction within this unit to be shorter than in compound **1U1**. We noted similar disparities in some of our Pb-oxo interactions and we believe these differences occur as a result of the angle of interaction.[27]

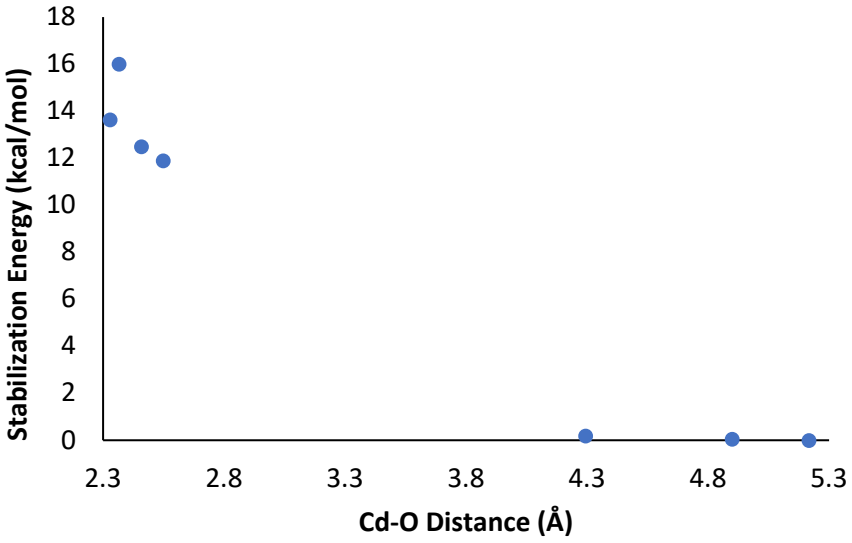

Figure 14. Cd-oxo distance vs total uranyl-cation interaction stabilization energy highlighting the relationship between distance and interaction strength between the UO_2^{2+} and the Cd^{2+} units.

We can contextualize these stabilization energies by comparing them to the analogous values calculated for the Pb^{2+}/UO_2^{2+} and Ag^{+}/UO_2^{2+} compounds (Figure S12). The Cd and Pb-oxo interactions have stabilization energies much higher than those for the Ag^{+}, likely as a result of the higher charge density on these metal cations. The Cd-oxo stabilization energy values are slightly lower than those for the Pb^{2+}-containing compounds. These results are in contrast with the more significant effects seen in the spectroscopy and bonding. Considering that SOPT is an orbital overlap-based method, there may be electrostatic differences between these cations that may not be fully accounted for. As such, this may reveal a shortcoming within the computational methods used to characterize the strength of these interactions.

Inner Sphere U=O Bonding. The bond critical point electron densities calculated by Quantum Theory of Atoms in Molecules (QTAIM) give a measure of the shared electrons between two atoms where higher electron density values indicate greater sharing and therefore indicate a stronger, more covalent bond.[42,55] The electron density (ρ) values as calculated by QTAIM for the

Cd-O interactions and the U=O bonds in **1-5** are summarized in Table 5. A typical ρ_{bcp} value for an unperturbed U=O bond is generally found between 0.300 and 0.320. For compounds **3-5** and for the U=O bonds in **1** and **2** that do not interact closely with the Cd^{2+}, the ρ_{bcp} values all fall close to this range. For the U=O bonds interacting closely with the Cd^{2+}, we see a significant decrease in the ρ_{bcp} to <0.280. These values are consistent with the bond asymmetry noted in the structural data. The ρ_{bcp} values for the Cd, Pb, and Ag containing compounds trend with the hardness of the metal cations. Taking Cd^{2+}/UO_2^{2+} compound **3** and representative Pb^{2+}/UO_2^{2+} and Ag^{+}/UO_2^{2+} compounds with comparable %vdW distances of 81%, 81% and 82% respectively, we see U=O ρ_{bcp} of 0.277, 0.0289, and 0.0307;[26,27] a clear trend in U=O bond weakening and loss of covalent character as a function of metal hardness.

Table 5. Quantum Theory of Atom in Molecules calculated bond critical point electron densities (ρ)

	U=O (Cd)	U=O	Cd-O
1U1	0.273	0.300	0.043
1U2	0.273	0.308	0.046
2U1	0.277	0.299	0.035
2U3	0.279	0.303	0.028
3	0.299	0.312	0.000
4	0.312	0.312	0.000
5	0.308	0.299	0.000

We also tabulate the ρ_{bcp} between the Cd and the uranyl oxo group (Table 5). For compounds **3-5** there is no electron density found between these two atoms but in **1** and **2** we see values ranging from 0.028 to 0.046. Pb-oxo interactions, in comparison, had ρ_{bcp} values with a maximum value of 0.020 and the Ag-oxo interactions had a maximum value of 0.034. We had previously rationalized the higher ρ_{bcp} value of the Ag-oxo interaction compared to the Pb-oxo interaction occurring because of the more charge dense Pb^{2+} favoring more electrostatic rather than covalent interactions. If that were the case, we would expect the even more charge dense Cd^{2+} cation to have *lower* ρ_{bcp} values than either of the other metals. As such we must revisit our previous conclusions. It is possible that the greater electron density at the bond critical points for oxo interactions with Cd^{2+} and Ag^{+} vs Pb^{2+}occurs as a result of the differing electron configurations.

Equatorial Effects

Throughout our studies of M^{n+}-oxo interactions, we have been cognizant of the reports from others that the effects of equatorial coordination on the uranyl bond and how this can, along with the M^{n+}-oxo interactions, have an effect on U=O bond strength and covalent character.[19,42,43,56] As such, our synthetic efforts aimed to keep the coordination sphere around the uranyl cation as similar as possible by using primarily carboxylate coordinating ligands. Despite best intentions, differences in coordination sphere were inevitable. Coordination with the

dipicolinate ligand and derivatives lead to an additional N-donor group. Even within purely carboxylate donor groups, we saw variability in coordination modes – sometimes monodentate coordination, other times bidentate chelating. And across the compounds, we saw a split of 7-coordinate and 8-coordinate coordination spheres around the uranium. Additionally, smaller differences in electron donation ability between ligands are also present.

In our previous work,[26,27] it was difficult to draw broader conclusions about the effects of equatorial coordination on metal-oxo interactions as we did not have large datasets for each metal, in particular since the Ag^{+}/UO_2^{2+} compounds (for which we had the largest dataset) do not display significant trends to track. With the addition of this work we can now compare within the 6 Pb^{2+}/UO_2^{2+} compounds previously published and the 5 Cd^{2+}/UO_2^{2+} compounds (in addition to the 12 compounds published by Thuéry that supplemented the Pb^{2+}/UO_2^{2+} paper[57–61]). Using this larger data set we can compare equatorial coordination between compounds with strong vs weak interactions (those that display spectroscopic changes vs those that do not).

We can compare the coordination number of these compounds to the strength of the interaction calculated by SOPT. In the compounds with multiple unique uranyl centers, the coordination number is the same for all the uranium centers, except in the case of compound **3** where one is 8-coordinate and the other is 7-coordinate. In this case, as the 8-coordinate uranium center is the one that interacts more closely with the Cd^{2+} (albeit still at 141%vdW), this is the center that was included for analysis. Of the compounds with stronger interactions there is a preference towards 7-coordinate with one exception being an 8-coordinate Pb^{2+}/UO_2^{2+} compound published by Thuéry (Refcode: GAPPEV) (Figure 15).[58] Conversely the 8-coordinate uranium centers seemed to favor weaker, longer interactions with two 7-coordinate exceptions one Pb^{2+} (Refcode: AYAVAZ)[61] and one Cd^{2+} (Compound **5**). This suggests a propensity within our dataset towards the formation of M^{n+}-oxo interactions in compounds with 7-coordinate uranyl complexes.

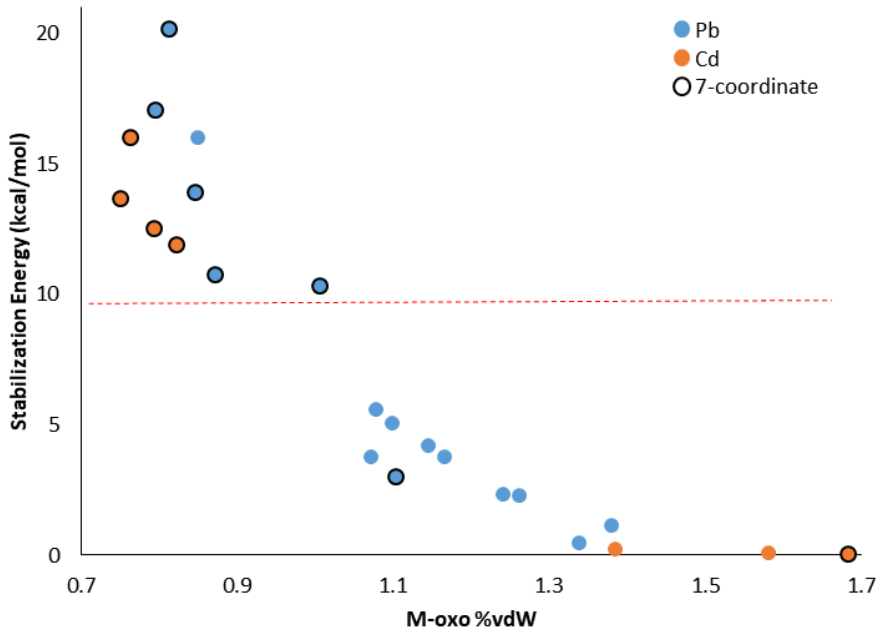

Figure 15. SOPT calculated stabilization energies for Cd^{2+}/UO_2^{2+} and Pb^{2+}/UO_2^{2+} compounds. Compounds circled with black are 7-coordinate, those not circled are 8-coordinate with respect to uranium. Compounds above the red, dotted line display significant spectroscopic changes as a result of M^{n+}-oxo interactions.

Generally speaking, in order for interactions to form, there must be an electronic attraction as well as favorable sterics. As such, we look at both of these factors in turn to determine which is the leading factor is within our compounds. We first analyzed the steric hindrance around the oxo groups using SambVca 2.1, to calculate the occupied volume around the oxo groups interacting closely with the metal cations (Table S1).[51] We found no correlation between percent buried volume values around the oxo group and equatorial coordination number nor the closeness of the axial M^{n+}-oxo interactions. As such, we do not believe that steric hindrance is the main factor in the formation of these interactions.

We moved on to analyze the electronic contributions within these interactions. An analysis of the QTAIM calculated charges of the UO_2^{2+} cation as a whole and the oxo groups, revealed a trend of greater negative charge on the uranyl cation and subsequently the uranyl oxo groups for the 7-coordinate compounds as compared to the 8-coordinate compounds (Figure 16). Likely the observed preference for oxo-interactions in the 7-coordinate compounds occurs as a result of more negative charge on the oxo group making interactions with the metal cations more favorable. These results suggest that tuning equatorial coordination number may help promote oxo-interactions.

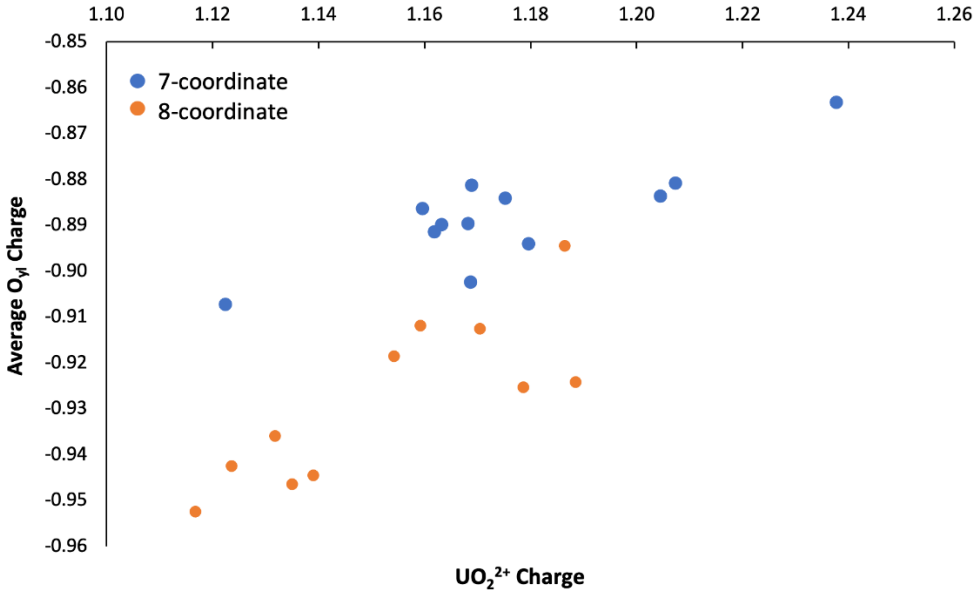

Figure 16. Sum of QTAIM calculated charge of UO_2^{2+} vs average of charge on the oxo groups in Cd^{2+}/UO_2^{2+} and Pb^{2+}/UO_2^{2+} compounds.

Conclusion

The syntheses and characterization of five novel Cd^{2+}/UO_2^{2+} heterometallic complexes have been described. Structural data revealed Cd-oxo interactions with distances ranging from

78% to 171% of the sum of the Van der Waals radii for these atoms. In the compounds displaying close interactions (<100% vdW), we observed quenched luminescence and lower energy asymmetric uranyl stretches in the Raman spectra. SOPT calculations found stronger stabilization energies as a result of closer interactions and QTAIM indicated a loss in covalent character in the U=O bonds as a result of these closer interactions. A comparison of these results to our Pb^{2+} and Ag^{+} materials revealed stronger effects of the Cd^{2+} cation experimentally and computationally, likely as a result of the increased hardness of this metal cation. For the SOPT results, which do not take electrostatic interactions into account, the Cd^{2+} had *lower* stabilization energies than the Pb^{2+} cation. This indicates that the charge transfer component of the interaction may be higher for the Pb^{2+} compounds, but that the higher electrostatic interactions of the Cd^{2+} cation are likely what causes the more significant effects seen in the experimental data.

An analysis of the equatorial coordination sphere of these compounds revealed a dependence of uranium coordination number on the formation of M^{n+}-oxo interactions, where 7-coordinate compounds were more likely to feature closer, stronger interactions. Analysis of the steric hindrance around the oxo-group found no correlation with coordination number and steric hindrance. QTAIM analysis found that 7-coordinate compounds had more negative UO_2^{2+} and O_{yl} charges. This more negative charge on the oxo-groups is favorable for the formation of interactions with the metal cations, explaining the preference towards M^{n+}-oxo interaction in 7-coordinate compounds. This analysis opens a door for future studies regarding the effects of equatorial coordination on the formation of oxo interactions. The effects of equatorial coordination could be leveraged along with metal cation hardness to systematically tune U=O bond character.

Associated Content

Supporting Information

The Supporting Information is available XXXX. Crystallographic information on CCDC 2310852-2310856 can be obtained free of charge by e-mailing data_request@ccdc. cam.ac.uk or by contacting The Cambridge Crystallographic Data Centre, 12 Union Road, Cambridge, CB2 1EZ UK; Fax +44(0)1223-336033; http://www.ccdc.cam.ac.uk/data_reque st/cif.

Ortep Figures, PXRD data, DFT models, Sample Computational Input File, Additional Stabilization Energy Plots, SambVca data (pdf)

X-ray data for compound **1** (CIF)
X-ray data for compound **2** (CIF)
X-ray data for compound **3** (CIF)
X-ray data for compound **4** (CIF)
X-ray data for compound **5** (CIF)

Author Information

***Christopher L. Cahill** - Department of Chemistry, The George Washington University, Washington, DC 20052, United States; orcid.org/0000-0002-2015-3595;
Email: cahill@gwu.edu

Authors

Dominique M. Brager - Department of Chemistry, The George Washington University, Washington, DC 20052, United States; orcid.org/0000-0003-0694-0805;
Email: dbrager@gwu.edu

Ahan J. Panchal - Department of Chemistry, The George Washington University, Washington, DC 20052, United States; orcid.org/0009-0004-1214-4551;
Email: ahanpanch@gwmail.gwu.edu

Author Contributions
The manuscript was written with contributions from all authors.

Notes
The authors declare no competing financial interests.

Acknowledgment
This study was supported by the U.S. Department of Energy (DOE) – Chemical Sciences, Geosciences, and Biosciences Division, Office of Science, Office of Basic Energy Sciences, Heavy Elements Program, under grant number DE-FG02-05ER15736. The authors would like to thank Professor Karah Knope and Anamar Blanes of Georgetown University for providing Raman microscope time. We would also like to thank Dr. Allen Oliver of Notre Dame University for his help with structural refinement of Compound **2**.

References

(1) Arnold, P. L.; Love, J. B.; Patel, D. Pentavalent Uranyl Complexes. *Coord. Chem. Rev.* **2009**, *253* (15–16), 1973–1978. https://doi.org/10.1016/j.ccr.2009.03.014.

(2) Zachara, J. M.; Long, P. E.; Bargar, J.; Davis, J. A.; Fox, P.; Fredrickson, J. K.; Freshley, M. D.; Konopka, A. E.; Liu, C.; McKinley, J. P.; Rockhold, M. L.; Williams, K. H.; Yabusaki, S. B. Persistence of Uranium Groundwater Plumes: Contrasting Mechanisms at Two DOE Sites in the Groundwater–River Interaction Zone. *J. Contam. Hydrol.* **2013**, *147*, 45–72. https://doi.org/10.1016/j.jconhyd.2013.02.001.

(3) Denning, R. G. Electronic Structure and Bonding in Actinyl Ions and Their Analogs. *J. Phys. Chem. A* **2007**, *111* (20), 4125–4143. https://doi.org/10.1021/jp071061n.

(4) Baker, R. J. New Reactivity of the Uranyl(VI) Ion. *Chem. – A Eur. J.* **2012**, *18* (51), 16258–16271. https://doi.org/10.1002/chem.201203085.

(5) Bean, A. C.; Scott, B. L.; Albrecht-Schmitt, T. E.; Runde, W. Structural and Spectroscopic Trends in Actinyl Iodates of Uranium, Neptunium, and Plutonium. *Inorg. Chem.* **2003**, *42* (18), 5632–5636. https://doi.org/10.1021/ic0341688.

(6) Nyman, M.; Burns, P. C. A Comprehensive Comparison of Transition-Metal and Actinyl Polyoxometalates. *Chem. Soc. Rev.* **2012**, *41* (22), 7354–7367. https://doi.org/10.1039/c2cs35136f.

(7) Den Auwer, C.; Simoni, E.; Conradson, S.; Madic, C. Investigating Actinyl Oxo Cations by X-Ray Absorption Spectroscopy. *Eur. J. Inorg. Chem.* **2003**, *2003* (21), 3843–3859. https://doi.org/10.1002/ejic.200300093.

(8) Natrajan, L. S. *Developments in the Photophysics and Photochemistry of Actinide Ions and Their Coordination Compounds*; Elsevier, 2012; Vol. 256, pp 1583–1603. https://doi.org/10.1016/j.ccr.2012.03.029.

(9) Carter, K. P.; Kalaj, M.; McNeil, S.; Kerridge, A.; Schofield, M. H.; Ridenour, J. A.; Cahill, C. L. Structural, Spectroscopic, and Computational Evaluations of Cation–Cation and Halogen Bonding Interactions in Heterometallic Uranyl Hybrid Materials. *Inorg. Chem. Front.* **2021**. https://doi.org/10.1039/d0qi01319f.

(10) Yang, W.; Parker, T. G.; Sun, Z. M. Structural Chemistry of Uranium Phosphonates. *Coord. Chem. Rev.* **2015**, *303*, 86–109. https://doi.org/10.1016/j.ccr.2015.05.010.

(11) Jayasinghe, A. S.; Payne, M. K.; Forbes, T. Z. Synthesis and Characterization of Heterometallic Uranyl Pyridinedicarboxylate Compounds. *J. Solid State Chem.* **2017**, *254*, 25–31. https://doi.org/10.1016/j.jssc.2017.07.002.

(12) Wang, K. X.; Chen, J. S. Extended Structures and Physicochemical Properties of Uranyl-Organic Compounds. *Acc. Chem. Res.* **2011**, *44* (7), 531–540. https://doi.org/10.1021/ar200042t.

(13) Cahill, C. L.; Lill, D. T. de; Frisch, M. Homo- and Heterometallic Coordination Polymers from the f Elements. *CrystEngComm* **2006**, *9* (1), 15–26. https://doi.org/10.1039/b615696g.

(14) Loiseau, T.; Mihalcea, I.; Henry, N.; Volkringer, C. The Crystal Chemistry of Uranium Carboxylates. *Coordination Chemistry Reviews*. Elsevier May 1, 2014, pp 69–109. https://doi.org/10.1016/j.ccr.2013.08.038.

(15) Carter, K. P.; Kalaj, M.; Kerridge, A.; Cahill, C. L. Probing Hydrogen and Halogen-Oxo Interactions in Uranyl Coordination Polymers: A Combined Crystallographic and Computational Study. *CrystEngComm* **2018**, *20* (34), 4916–4925. https://doi.org/10.1039/C8CE00682B.

(16) Carter, K. P.; Kalaj, M.; Cahill, C. L. Harnessing Uranyl Oxo Atoms: Via Halogen Bonding Interactions in Molecular Uranyl Materials Featuring 2,5-Diiodobenzoic Acid and N-Donor Capping Ligands. *Inorg. Chem. Front.* **2017**, *4* (1), 65–78. https://doi.org/10.1039/c6qi00352d.

(17) Bell, N. L.; Arnold, P. L.; Love, J. B. Controlling Uranyl Oxo Group Interactions to Group 14 Elements Using Polypyrrolic Schiff-Base Macrocyclic Ligands. *Dalt. Trans.* **2016**, *45* (40), 15902–15909. https://doi.org/10.1039/c6dt01948j.

(18) Fortier, S.; Hayton, T. W. Oxo Ligand Functionalization in the Uranyl Ion (UO22+). *Coord. Chem. Rev.* **2010**, *254* (3–4), 197–214. https://doi.org/10.1016/j.ccr.2009.06.003.

(19) Yahia, A.; Arnold, P. L.; Love, J. B.; Maron, L. The Effect of the Equatorial Environment on Oxo-Group Silylation of the Uranyl Dication: A Computational Study. *Chem. – A Eur. J.* **2010**, *16* (16), 4881–4888. https://doi.org/10.1002/chem.200902991.

(20) Arnold, P. L.; Hollis, E.; White, F. J.; Magnani, N.; Caciuffo, R.; Love, J. B. Single-Electron Uranyl Reduction by a Rare-Earth Cation. *Angew. Chemie Int. Ed.* **2011**, *50* (4), 887–890. https://doi.org/10.1002/anie.201005511.

(21) Arnold, P. L.; Patel, D.; Blake, A. J.; Wilson, C.; Love, J. B. Selective Oxo Functionalization of the Uranyl Ion with 3d Metal Cations. *J. Am. Chem. Soc.* **2006**, *128* (30), 9610–9611. https://doi.org/10.1021/ja0634167.

(22) Arnold, P. L.; Pécharman, A.-F.; Lord, R. M.; Jones, G. M.; Hollis, E.; Nichol, G. S.; Maron, L.; Fang, J.; Davin, T.; Love, J. B. Control of Oxo-Group Functionalization and Reduction of the Uranyl Ion. *Inorg. Chem.* **2015**, *54* (7), 3702–3710. https://doi.org/10.1021/acs.inorgchem.5b00420.

(23) Arnold, P. L.; Pécharman, A.-F.; Hollis, E.; Yahia, A.; Maron, L.; Parsons, S.; Love, J. B. Uranyl Oxo Activation and Functionalization by Metal Cation Coordination. *Nat. Chem.* **2010**, *2* (12), 1056–1061. https://doi.org/10.1038/nchem.904.

(24) Arnold, P. L.; Cowie, B. E.; Arkøta Suvova, M.; Zegke, M.; Magnani, N.; Colineau, E.; Griveau, J.-C.; Caciuffo, R.; Love, J. B.; Arnold, P. L.; Owie, B. E. C.; Suvova, M.; Egke, M. Z.; Love, J. B.; Magnani, N.; Colineau, E.; Griveau, J.-C.; Caciuffo, R. Axially Symmetric U−O−Ln- and U−O−U-Containing Molecules from the Control of Uranyl Reduction with Simple f-Block Halides. *Angew. Chemie Int. Ed.* **2017**, *56* (36), 10775–10779. https://doi.org/10.1002/anie.201705197.

(25) Vitova, T.; Faizova, R.; Amaro-Estrada, J. I.; Maron, L.; Pruessmann, T.; Neill, T.; Beck, A.; Schacherl, B.; Tirani, F. F.; Mazzanti, M. The Mechanism of Fe Induced Bond Stability of Uranyl(V). *Chem. Sci.* **2022**, *13* (37), 11038–11047. https://doi.org/10.1039/d2sc03416f.

(26) Brager, D. M.; Marwitz, A. C.; Cahill, C. L. A Spectroscopic, Structural, and Computational Study of Ag-Oxo Interactions in Ag+/UO22+complexes. *Dalt. Trans.* **2022**, *51*, 10095–10120. https://doi.org/10.1039/D2DT01161A.

(27) Brager, D. M.; Nicholas, A. D.; Schofield, M. H.; Cahill, C. L. Pb-Oxo Interactions in Uranyl Hybrid Materials: A Combined Experimental and Computational Analysis of Bonding and Spectroscopic Properties. *Inorg. Chem.* **2021**, *60* (22), 17186–17200. https://doi.org/10.1021/acs.inorgchem.1c02518.

(28) Groom, C. R.; Bruno, I. J.; Lightfoot, M. P.; Ward, S. C. The Cambridge Structural Database. *Acta Crystallogr. Sect. B Struct. Sci. Cryst. Eng. Mater.* **2016**, *72* (2), 171–179.

https://doi.org/10.1107/S2052520616003954.

Search criteria: Structures including Pb and a uranyl unit (O=U=O)

(29) Bruker. APEXIII. Bruker AXS Inc.: Madison, Wisconsin, USA 2020.

(30) Bruker. BIS. Bruker AXS Inc.: Madison, Wisconsin, USA 2020.

(31) SAINT Version 8.34a. Bruker AXS Inc. Madison, WI, WI 2013.

(32) Sheldrick, G. M. SADABS. University of Göttingen: Göttingen, Germany 2005.

(33) Sheldrick, G. M. A Short History of SHELX. *Acta Crystallogr. Sect. A* **2008**, *64*, 112–122. https://doi.org/10.1107/s0108767307043930.

(34) Huebschle, C. B.; Sheldrick, G. M.; Dittrich, B. ShelXle: A Qt Graphical User Interface for SHELXL. *J. Appl. Crystallogr.* **2011**, *44* (6), 1281–1284. https://doi.org/10.1107/s0021889811043202.

(35) CrystalMaker, 8.2.2 Ed. Crystal Maker Software Limited: Bicester, England 2009.

(36) Putz, H. Match! Phase Identification from Powder Diffraction. Crystal Impact: Bonn, Germany.

(37) Glendening, E. D.; Reed, A. E.; Carpenter, J. E.; Bahmann, J. A.; Morales, C. M. NBO 7.0. University of Wisconsin-Madison: Theoretical Chemistry Institute 2018.

(38) King, R. B. Coordination Chemistry in Two Dimensions: The Angular Overlap Model for Actinyl Complexes. *J. Coord. Chem.* **2005**, *58* (1), 47–53. https://doi.org/10.1080/00958970512331327375.

(39) Frisch, M. J.; Trucks, G. W.; Schlegel, H. B.; Scuseria, G. E.; Robb, M. A.; Cheeseman, J. R.; Scalmani, G.; Barone, V.; Petersson, G. A.; Nakatsuji, H.; Li, X.; Caricato, M.; Marenich, A. V.; Bloino, J.; Janesko, B. G.; Gomperts, R.; Mennucci, B.; Hratchian, H. P.; Ortiz, J. V.; Izmaylov, A. F.; Sonnenberg, J. L.; Williams-Young, D.; Ding, F.; Lipparini, F.; Egidi, F.; Goings, J.; Peng, B.; Petrone, A.; Henderson, T.; Ranasinghe, D.; Zakrzewski, V. G.; Gao, J.; Rega, N.; Zheng, G.; Liang, W.; Hada, M.; Ehara, M.; Toyota, K.; Fukuda, R.; Hasegawa, J.; Ishida, M.; Nakajima, T.; Honda, Y.; Kitao, O.; Nakai, H.; Vreven, T.; Throssell, K.; Montgomery, J. A., J.; Peralta, J. E.; Ogliaro, F.; Bearpark, M. J.; Heyd, J. J.; Brothers, E. N.; Kudin, K. N.; Staroverov, V. N.; Keith, T. A.; Kobayashi, R.; Normand, J.; Raghavachari, K.; Rendell, A. P.; Burant, J. C.; Iyengar, S. S.; Tomasi, J.; Cossi, M.; Millam, J. M.; Klene, M.; Adamo, C.; Cammi, R.; Ochterski, J. W.; Martin, R. L.; Morokuma, K.; Farkas, O.; Foresman, J. B.; Fox, D. J. Gaussian 16, Revision B.01, Gaussian, Inc., Wallingford CT. **2016**.

(40) Weigend, F. Accurate Coulomb-Fitting Basis Sets for H to Rn. *Phys. Chem. Chem. Phys.* **2006**, *8* (9), 1057. https://doi.org/10.1039/B515623H.

(41) Becke, A. D. Density-Functional Thermochemistry. III. The Role of Exact Exchange. *J. Chem. Phys.* **1993**, *98* (7), 5648–5652. https://doi.org/10.1063/1.464913.

(42) Di Pietro, P.; Kerridge, A.; Pietro, P. Di; Kerridge, A. U–Oyl Stretching Vibrations as a Quantitative Measure of the Equatorial Bond Covalency in Uranyl Complexes: A

Quantum-Chemical Investigation. *Inorg. Chem.* **2016**, *55* (2), 573–583. https://doi.org/10.1021/acs.inorgchem.5b01219.

(43) Di Pietro, P.; Kerridge, A.; Pietro, P. Di; Kerridge, A. Assessing Covalency in Equatorial U–N Bonds: Density Based Measures of Bonding in BTP and Isoamethyrin Complexes of Uranyl. *Phys. Chem. Chem. Phys.* **2016**, *18* (25), 16830–16839. https://doi.org/10.1039/c6cp01273f.

(44) Krishnan, R.; Binkley, J. S.; Seeger, R.; Pople, J. A. Self-consistent Molecular Orbital Methods. XX. A Basis Set for Correlated Wave Functions. *J. Chem. Phys.* **1980**, *72* (1), 650–654. https://doi.org/10.1063/1.438955.

(45) Weigend, F.; Ahlrichs, R. Balanced Basis Sets of Split Valence, Triple Zeta Valence and Quadruple Zeta Valence Quality for H to Rn: Design and Assessment of Accuracy. *Phys. Chem. Chem. Phys.* **2005**, *7* (18), 3297. https://doi.org/10.1039/B508541A.

(46) Cao, X.; Dolg, M.; Stoll, H. Valence Basis Sets for Relativistic Energy-Consistent Small-Core Actinide Pseudopotentials. *J. Chem. Phys.* **2003**, *118* (2), 487. https://doi.org/10.1063/1.1521431.

(47) Cao, X.; Dolg, M. J. Segmented Contraction Scheme for Small-Core Actinide Pseudopotential Basis Sets. *Molec. Struct. (Theochem)* **2004**, *673* (1–3), 203. https://doi.org/10.1016/j.theochem.2003.12.015.

(48) Kuechle, W.; Dolg, M.; Stoll, H.; Preuss, H.; Küchle, W.; Dolg, M.; Stoll, H.; Preuss, H. Energy-adjusted Pseudopotentials for the Actinides. Parameter Sets and Test Calculations for Thorium and Thorium Monoxide. *J. Chem. Phys.* **1994**, *100* (10), 7535. https://doi.org/10.1063/1.466847.

(49) Bader, R. F. W. *Atoms in Molecules: A Quantum Theory*; Oxford University Press: Oxford, UK, 1990.

(50) Keith, T. A. AIMAll, Version 19.10.12. TK Gristmall Software: Overland Park, Kansas, USA 2019.

(51) Falivene, L.; Cao, Z.; Petta, A.; Serra, L.; Poater, A.; Oliva, R.; Scarano, V.; Cavallo, L. Towards the Online Computer-Aided Design of Catalytic Pockets. *Nat. Chem.* **2019**, *11* (10), 872–879. https://doi.org/10.1038/s41557-019-0319-5.

(52) Bondi, A. Van Der Waals Volumes and Radii. *J. Phys. Chem.* **1964**, *68* (3), 441–451. https://doi.org/10.1021/j100785a001.

(53) Lu, G.; Haes, A. J.; Forbes, T. Z. Detection and Identification of Solids, Surfaces, and Solutions of Uranium Using Vibrational Spectroscopy. *Coord. Chem. Rev.* **2018**, *374*, 314–344. https://doi.org/10.1016/j.ccr.2018.07.010.

(54) Surbella, R. G.; Cahill, C. L. The Exploration of Supramolecular Interactions Stemming from the [UO 2(NCS)4(H2O)]2- Tecton and Substituted Pyridinium Cations. *CrystEngComm* **2014**, *16* (12), 2352–2364. https://doi.org/10.1039/c3ce42106f.

(55) A. Kerridge. Quantification of F-Element Covalency through Analysis of the Electron Density: Insights from Simulation. *Chem. Commun.* **2017**, *53* (50), 6685–6695.

https://doi.org/10.1039/c7cc00962c.

(56) Bell, N. L.; Shaw, B.; Arnold, P. L.; Love, J. B. Uranyl to Uranium(IV) Conversion through Manipulation of Axial and Equatorial Ligands. *J. Am. Chem. Soc.* **2018**, *140* (9), 3378–3384. https://doi.org/https://doi.org/10.1021/jacs.7b13474.

(57) Thuéry, P.; Harrowfield, J. Variations on the Honeycomb Topology: From Triangular- and Square-Grooved Networks to Tubular Assemblies in Uranyl Tricarballylate Complexes. *Cryst. Growth Des.* **2017**, *17* (3), 963–966. https://doi.org/10.1021/acs.cgd.7b00126.

(58) Thuéry, P.; Harrowfield, J. AgI and PbII as Additional Assembling Cations in Uranyl Coordination Polymers and Frameworks. *Cryst. Growth Des.* **2017**, *17* (4), 2116–2130. https://doi.org/10.1021/acs.cgd.7b00081.

(59) Thuéry, P.; Harrowfield, J. Structural Consequences of 1,4-Cyclohexanedicarboxylate Cis/Trans Isomerism in Uranyl Ion Complexes: From Molecular Species to 2D and 3D Entangled Nets. *Inorg. Chem.* **2017**, *56* (21), 13464–13481. https://doi.org/10.1021/acs.inorgchem.7b02176.

(60) Thuéry, P.; Harrowfield, J. Modulation of the Structure and Properties of Uranyl Ion Coordination Polymers Derived from 1,3,5-Benzenetriacetate by Incorporation of Ag(I) or Pb(II). *Inorg. Chem.* **2016**, *55* (13), 6799–6816. https://doi.org/10.1021/acs.inorgchem.6b01168.

(61) Thuéry, P.; Harrowfield, J. Tetrahydrofurantetracarboxylic Acid: An Isomerizable Framework-Forming Ligand in Homo- and Heterometallic Complexes with UO22+, Ag+, and Pb2+. *Cryst. Growth Des.* **2016**, *16* (12), 7083–7093. https://doi.org/10.1021/acs.cgd.6b01312.

Synopsis:

Cd2+ interactions with the uranyl oxo lead to significant U=O bond weakening evidenced in stuctural and Raman spectroscopic data. The bond weakening occurs as a result of charge transfer between U=O bonding and antibonding orbitals and the Cd2+ cation. These interactions are more significant than the previously reported Pb2+-oxo and Ag+-oxo interactions. Additonally, equatorial coordination number is shown influence the propensity of the uranyl cation towards forming oxo interactions with metal cations.